MS: for BBB

Title: The role of calcium binding to the EF-hand-like motif in bacterial solute-binding protein for alginate import

Running Head: Bacterial alginate-binding protein

Authors: Kenji Okumura[1], Yukie Maruyama[2], Ryuichi Takase[1], Bunzo Mikami[3], Kousaku Murata[2], and Wataru Hashimoto[1,]*

Affiliations: [1]Laboratory of Basic and Applied Molecular Biotechnology, Division of Food Science and Biotechnology, Graduate School of Agriculture, Kyoto University, Uji, Kyoto 611-0011, Japan. [2]Laboratory of Food Microbiology, Department of Life Science, Faculty of Science and Engineering, Setsunan University, Neyagawa, Osaka 572-8508, Japan. [3]Laboratory of Metabolic Sciences of Forest Plants and Microorganisms, Research Institute for Sustainable Humanosphere, Kyoto University, Uji, Kyoto 611-0011, Japan.

*Correspondence: Wataru Hashimoto, hashimoto.wataru.8c@kyoto-u.ac.jp

Abstract (146/150 words)

Gram-negative *Sphingomonas* sp. A1 incorporates acidic polysaccharide alginate into the cytoplasm *via* a cell-surface alginate-binding protein (AlgQ2)-dependent ATP-binding cassette transporter (AlgM1M2SS). We investigated the function of calcium bound to the EF-hand-like motif in AlgQ2 by introducing mutations at the calcium-binding site. The X-ray crystallography of the AlgQ2 mutant (D179A/E180A) demonstrated the absence

of calcium binding and significant disorder of the EF-hand-like motif. Distinct from the wild-type AlgQ2, the mutant was quite unstable at temperature of strain A1 growth, although unsaturated alginate oligosaccharides stabilized the mutant by formation of substrate/protein complex. In the assay of ATPase and alginate transport by AlgM1M2SS reconstructed in the liposome, the wild-type and mutant AlgQ2 induced AlgM1M2SS ATPase activity in the presence of unsaturated alginate tetrasaccharide. These results indicate that the calcium bound to EF-hand-like motif stabilizes the substrate-unbound AlgQ2 but is not required for the complexation of substrate-bound AlgQ2 and AlgM1M2SS.

Keywords

ABC transporter, calcium, EF-hand-like motif, solute-binding protein, X-ray crystallography

Introduction

ATP-binding cassette (ABC) transporters require the energy generated *via* ATP hydrolysis (ATPase) to translocate a variety of molecules across the cytoplasmic membrane (Davidson *et al*. 2008). ABC transporters can be either importers or exporters. ABC importers are mainly produced by prokaryotes, whereas ABC exporters are present in all species (Locher 2008). Bacterial ABC importers are classified into three types: type I, type II, and type III (Rice *et al*. 2014). Type I and II ABC importers require solute-binding protein (SBP) to transport substrate (Oldham *et al*. 2008). SBP consists of two large domains that are connected by hinge loops and adopts two conformations, namely, an open substrate-unbound conformation and a closed substrate-bound conformation

(Tang *et al*. 2007). ABC transporters are composed of two transmembrane domains (TMD) and two nucleotide-binding domains (NBD). ATPase activity by an NBD causes the TMD to change conformation from inward-facing to outward-facing. It is important for the substrate transport in order to alter the structural conformation (ter Beek *et al*. 2014).

Although SBPs were classified into six clusters based on structural features (Berntsson *et al*. 2010), a new seventh SBP cluster, characterized by an EF-hand-like calcium-binding motif has been proposed (Scheepers *et al*. 2016). Similarity in sequence and structure is observed among SBPs assigned to the seventh cluster, while there is little similarity between the seventh cluster and other clusters. The EF-hand-like helix–loop–strand motif in SBPs of the seventh cluster has a metal-binding loop that consists of nine amino acid residues, and is located near the SBP-TMD interaction surface. FusA, the SBP for fructooligosaccharide import in *Streptococcus pneumoniae*, is a member of the new SBP cluster identified by its EF-hand-like motif (Culurgioni *et al*. 2017). Mutations in the calcium-binding residues of the FusA EF-hand-like motif render *S. pneumoniae* unable to grow on nystose, a fructotetrasaccharide, as a sole carbon source. This result indicates that EF-hand-like motif-bound calcium is important for fructooligosaccharide import (Culurgioni *et al*. 2017).

Alginate is an acidic polysaccharide that consists of β-D-mannuronate (M) and α-L-guluronate (G) (Gacesa 1988). The gram-negative *Sphingomonas* sp. A1 (strain A1) directly incorporates the alginate polymer through the cell-surface pit (Hisano *et al*. 1996). The periplasmic SBP (AlgQ1 or AlgQ2) and inner-membrane ABC transporter (AlgM1M2SS) cooperatively transport alginate from periplasm to cytoplasm across the inner membrane (Momma *et al*. 2000). AlgM1 and AlgM2 correspond to the TMD, and

two AlgS molecules correspond to the NBD. AlgQ1 and AlgQ2 are mutually similar (sequence identity: 76%), and both bind alginate and pass the polymer to AlgM1M2SS at the same level (Nishitani *et al*. 2012). AlgQ1 or AlgQ2 binds alginate to form a closed conformation, and alginate-bound AlgQ1 or AlgQ2 interacts with AlgM1M2SS to enhance ATPase activity by AlgS (Kaneko *et al*. 2017). Both AlgQ1 and AlgQ2 have an EF-hand-like calcium-binding motif. In the complex structure of AlgQ2 and AlgM1M2SS, the EF-hand-like motif is located near the interface between AlgQ2 and AlgM2 (Figure 1a) (Maruyama *et al*. 2015), suggesting that calcium bound to the EF-hand-like motif plays a significant role in the interaction between AlgQ2 and AlgM1M2SS (Culurgioni *et al*. 2017).

The EF-hand motif has a helix–loop–helix conformation in which two helices lie in near-parallel arrangement, and the calcium ions are coordinated by residues within a loop. The representative EF-hand loop is composed of 12 amino acid residues and is called canonical EF-hand loop. There are variations in the length of the loop from 9 to 15 residues (Gifford *et al*. 2007, Delfina *et al*. 2015). Due to these variations, EF-hand-like motif is postulated. The EF-hand-like motif of SBPs in the seventh cluster has a metal-binding loop consisting of nine amino acid residues. Calcium in the calmodulin EF hand is known to function in signal transduction or protein interaction (Carafoli 2002; Ababou and Zaleska 2002). However, the role of calcium bound to the EF-hand-like motif in SBP interacting with ABC transporter remains unclear. This paper provides a structural and functional characterization of calcium-unbound SBP (AlgQ2) *via* X-ray crystallography and *in vitro* assay using ABC transporter (AlgM1M2SS) in liposomes.

Materials and methods

Preparation of alginate oligosaccharides

Sodium alginate (Nacalai Tesque, Extra Pure Reagent grade, product No. 31132-75) was treated with 0.1 mg/mL of endolytic poly(mannuronate) alginate lyase from *Flavobacterium* (Sigma-Aldrich) for 30 min at 25°C. The products were separated *via* anion-exchange chromatography [TOYOPEARL DEAE-650M (Tosoh)] and eluted with a gradient of ammonium bicarbonate 0 to 1 M. The oligosaccharide length was confirmed *via* thin-layer chromatography using standard markers. After lyophilization, the unsaturated alginate trisaccharide was dissolved in distilled water.

Unsaturated tetramannuronate Δ4M substrate was prepared from alginate as reported (Nishitani *et al*. 2012). To prepare PAΔ4M, Δ4M was labeled with 2-aminopyridine and purified *via* column chromatography as reported (Maruyama *et al*. 2015).

Site-directed mutagenesis of AlgQ2

To introduce alanine substitution in Asp179 and Glu180, inverse PCR was performed using a vector (pAQ2) used for *Escherichia coli* AlgQ2 expression (Momma *et al*. 2002) as a template, synthetic oligonucleotide DNA as a primer (Forward: GGCAACGGCAAGGCCGCTGCAATTCCGTTCATCAAC, Reverse: GTTGATGAACGGAATTGCAGCGGCCTTGCCGTTGCC; the mutation sites are underlined), and KOD FX Neo (TOYOBO) as a DNA polymerase. The PCR product was treated with *Dpn*I and used to transform *E. coli* BL21(DE3)pLysS. *E. coli* BL21(DE3)pLysS cells harboring mutant pAQ2 were grown in LB medium containing 100 μg/mL of sodium ampicillin, collected *via* centrifugation at 4,000 *g* and 4°C for 20 min, and resuspended in 20-mM potassium phosphate buffer (pH 6.8). The cells were ultrasonically disrupted (201M Insonator, Kubota) at 0°C for 20 min, and cell extract was obtained *via* centrifugation at 15,000 *g* for 20 min. The cell extract was dialyzed against

20-mM potassium phosphate buffer (pH 6.8) and applied to a TOYOPEARL SP-650 M (Tosoh). The protein was eluted with a linear gradient of 0–0.5 M NaCl. The fractions containing the protein were dialyzed against 20-mM Tris-HCl buffer (pH 7.5). AlgQ2 wild-type (wtAlgQ2) was purified in the same procedure as mutant AlgQ2 (mtAlgQ2). All procedures were performed at 0°C–4°C.

Quantitative analysis of calcium with inductively coupled plasma (ICP)

Purified wtAlgQ2 and mtAlgQ2 were diluted with 20-mM Tris-HCl (pH 7.5) to a concentration of 10 μM determined based on the extinction coefficient calculated by the primary structure of AlgQ2 (the protein concentration was approximately determined to 1 mg/mL when the absorbance at 280 nm of the protein solution showed 2). Nitric acid (2 mL) was added to 2 mL of each sample and applied to microwave digestion with UltraWAVE (Milestone General). The samples were allowed to cool and messed up with ultrapure water. These samples were applied to an ICP emission spectrometer (ICPS-8100, Shimadzu) to quantify calcium concentration.

X-ray crystallography of mtAlgQ2

mtAlgQ2 crystallization was performed in the presence of unsaturated alginate trisaccharide using the sitting-drop vapor diffusion method at 20°C for several weeks. mtAlgQ2 mixed with unsaturated alginate trisaccharide substrate was crystallized in 0.2 M sodium formate, 0.1 M 1,3-bis[tris(hydroxymethyl)methylamino]propane (pH 8.5), and 20% polyethylene glycol 3350. A crystal was picked up using a mounted nylon loop (Hampton Research) and placed directly into a cold nitrogen gas stream at −173°C. For cryoprotection, a protein crystal was soaked in the reservoir solution containing 20% glycerol. The diffraction data were collected at a wavelength of 1.0000 Å using a MAR225HE detector at BL38B1 beamline in SPring-8 (Hyogo, Japan) and processed

with *HKL2000* (Otwinowski and Minor 1997). The structure was solved by molecular replacement using *Molrep* (Vagin and Teplyakov 1997) with the coordinates of wtAlgQ2 (PDB ID: 1J1N) as an initial search model and refined with *Refmac5* (Murshudov *et al*. 1997). The *winCoot* program (Emsley and Cowtan 2004) was utilized for model modification. To build the ligand, preinstalled coordinates and cif dictionaries were used in *winCoot*. The final model was evaluated using *PROCHECK* (Laskowski *et al*. 1993). The figures were prepared using *Pymol* (Schrodinger 2010). The atomic coordinates and structure factors (code 6JHX for mtAlgQ2) were deposited in the Protein Data Bank, Research Collaboratory for Structural Bioinformatics, Rutgers University, New Brunswick, NJ (http://www.rcsb.org/).

Differential scanning fluorimetry (DSF) analysis

The thermal stability of wtAlgQ2 and mtAlgQ2 in the presence or absence of 20-μM $CaCl_2$ and/or 50-μM Δ4M was investigated *via* DSF (Niesen *et al*. 2007). This experiment was conducted using a real-time PCR instrument (MyiQ2, Bio-Rad). The reaction mixture consisted of 1.7 μM of wtAlgQ2 or mtAlgQ2, 60-fold diluted SYPRO Orange (Invitrogen), and 20-mM Tris-HCl (pH 7.5). The reaction mixtures were subjected to heat treatment, and the temperature was increased from 25°C to 95°C by 0.5°C/cycle (10 s/cycle) for 141 cycles. Fluorescence emitted from SYPRO Orange bound to denatured protein was measured by excitation at 492 nm and emission at 610 nm. Apparent melting temperature (T_m) was calculated as the midpoint of increase in the fluorescence profile. The fluorescence profile was analyzed with *iQ5* (Bio-Rad) to determine the apparent T_m.

Native PAGE

Native PAGE was performed to examine the binding affinity of wtAlgQ2 or mtAlgQ2 with Δ4M. wtAlgQ2 or mtAlgQ2 (17 μM) was mixed with 0- to 22-μM Δ4M at 4°C to

avoid denaturation of mtAlgQ2. Electrophoresis was performed at 4°C and 10 mA for 2 h using 5% polyacrylamide gel and a running buffer consisting of 43-mM imidazole and 35-mM 4-(2-hydroxyethyl)-1-piperazineethanesulfonic acid (HEPES) (pH 7.4) (McLellan 1982) without heat pretreatment. The protein band densities on the gel were quantified using *ImageJ* (Schneider *et al*. 2012).

ATPase activity of AlgM1M2SS

Expression and purification of AlgM1M2SS [AlgM1(d0)M2(H10)SS(WT)], in which 10 histidine residues were added to the C terminus of AlgM2, were conducted as described (Maruyama *et al*. 2015). AlgM1M2SS was reconstructed in the liposome produced by L-α-phosphatidylcholine Type IV-S (Sigma-Aldrich) derived from soybean (Maruyama *et al*. 2015). The ATPase activity of the proteoliposome was measured in 200 μL of reaction mixtures containing 0.1-μM AlgM1M2SS reconstituted in the liposome, 5-mM $MgCl_2$, 5-mM ATP, 20-mM Tris-HCl (pH 8.0), 20-μM Δ4M or PAΔ4M, and 1-μM AlgQ2. The reaction mixtures were incubated at 37°C. The samples (30 μL) were collected from the reaction mixture at various times and added to 30 μL of 12% sodium dodecyl sulfate to stop the reaction. Inorganic phosphate was quantified *via* phosphomolybdic acid colorimetry (Chifflet *et al*. 1998). ATPase activity was measured as inorganic phosphate per min, and the same experiment was conducted in the absence of AlgM1M2SS.

Alginate transport activity

AlgM1M2SS was reconstructed in the liposome produced by L-α-phosphatidylcholine Type II-S (Sigma-Aldrich) derived from soybean as reported (Maruyama *et al*. 2015). To prepare ATP and $MgCl_2$ containing the proteoliposome, the mixture of proteoliposome, ATP, and $MgCl_2$ was freeze-thawed three times with liquid nitrogen and a water bath, followed by Nuclepore membrane (Whatman, pore size of 0.1 μm) filtration using a Mini-

193 Extruder (Avanti Polar Lipids). Alginate transport activity was measured in 200-μL
194 reaction mixtures containing 0.1-μM AlgM1M2SS reconstituted in liposomes, 1-mM
195 $MgCl_2$, 5-mM ATP, 20-mM Tris-HCl (pH 8.0), 20-μM PAΔ4M, and 1-μM AlgQ2. The
196 reaction mixtures were incubated at 37°C for 1 h. After the reaction, the proteoliposome
197 was collected *via* ultracentrifugation (4°C, 192,000 g, 30 min). The collected liposomes
198 were diluted in pure water and disrupted by vortexing. The concentration of PAΔ4M was
199 calculated from the fluorescence intensity (Ex, 310 nm; Em, 380 nm). Liposomes without
200 AlgM1M2SS were reacted in 20-μM PAΔ4M and 1-μM wtAlgQ2 or mtAlgQ2 to subtract
201 the values of the AlgM1M2SS transport activity under each condition. In the negative
202 control [AlgQ2(−)/PAΔ4M(+) and AlgQ2(−)/PAΔ4M(−)], the mean value of the
203 observed transport activity in liposomes without AlgM1M2SS in the presence of
204 wtAlgQ2 and mtAlgQ2 was subtracted.
205
206 **Results**
207 **Mutations at the EF-hand-like calcium-binding site**
208 The crystal structure of AlgQ2 was described elsewhere (Momma *et al*. 2002). Five
209 amino acid residues (Asn173, Asn175, Lys177, Asp179, and Glu180) coordinate calcium
210 at the EF-hand-like motif of AlgQ2 (Figure 1b). mtAlgQ2 was constructed by replacing
211 two (Asp179 and Glu180) of the five residues with alanine to disrupt the calcium-binding
212 ability of the EF-hand-like motif. Recombinant wtAlgQ2 and mtAlgQ2 were expressed
213 in *E. coli* and purified to homogeneity *via* column chromatography. The calcium
214 concentration of each protein solution was quantified *via* ICP emission spectroscopy
215 (Table 1). The amounts of calcium and protein were comparable in the wtAlgQ2 solution,
216 whereas the calcium concentration was drastically reduced to 10% of the protein

concentration in the mtAlgQ2 solution. This result indicated that the mutations in calcium-coordinated amino acid residues dramatically reduced the affinity of AlgQ2 for calcium, as predicted.

Crystal structure of calcium-unbound mtAlgQ2 in complex with substrate

To obtain structural insights into the role of calcium at EF-hand-like motif, the mtAlgQ2 structure was determined *via* X-ray crystallography. The crystal of mtAlgQ2 was subjected to X-ray diffraction experiments. The statistics for data collection and structure refinement are summarized in Table 2.

The structure of mtAlgQ2 in complex with alginate trisaccharide was determined at 2.2 Å resolution (Figure 2a). No calcium was detected at the EF-hand-like motif in the crystal structure. Due to the unclear electron density map around the EF-hand-like motif loop, the residues (174–178) in the motif were omitted from the coordinates (Figure 2b). The results indicated that the mutations caused local loop destabilization. The structural identity between wtAlgQ2 and mtAlgQ2 was evaluated by superimposing the coordinates of two proteins (wtAlgQ2, PDB ID: 5H71) using the *ASH* program (Toh 1997; Standley *et al*. 2004) (Figure 2c). The global root-mean-square deviation (RMSD) was 0.47 Å for all Cα atoms, indicating that the mutations and/or the absence of calcium exerted a negligible effect on the overall structure, except for the local conformation of the EF-hand-like motif loop.

Extreme destabilization of substrate-unbound mtAlgQ2

The thermal stability of wtAlgQ2 and mtAlgQ2 was examined *via* DSF (Niesen *et al*. 2007). The fluorescence intensity derived from SYPRO Orange bound to denatured protein was measured *via* a melting curve analysis using a real-time PCR instrument. wtAlgQ2 in the absence of substrate, unsaturated tetramannuronate (Δ4M), demonstrated

241 an apparent T_m of 45.6°C (Figure 3, red). mtAlgQ2 in the absence of Δ4M emitted intense
242 fluorescence at 25°C (Figure 3, blue), indicating that mtAlgQ2 was denatured at 25°C or
243 less. In the presence of Δ4M at 50 μM, the wtAlgQ2 apparent T_m increased to 63.2°C
244 (Figure 3 black) (Nishitani *et al*. 2012), and mtAlgQ2 was stabilized to an apparent T_m of
245 55.7°C (Figure 3, green). These results indicated that both wtAlgQ2 and mtAlgQ2 were
246 stabilized by forming a complex with alginate oligosaccharide and that mtAlgQ2 adopts
247 an extremely unstable substrate-unbound form (open conformation) and stable substrate-
248 bound form (closed conformation). Calcium bound to the EF-hand-like motif is, therefore,
249 crucial for the stabilization of substrate-unbound form. Conversely, the additional
250 calcium in the reaction mixture at 20 μM, about 10 times the concentration of protein (1.7
251 μM), had a negligible effect on the stability of both proteins in the presence or absence
252 of Δ4M (Table 3).

253 **mtAlgQ2 and wtAlgQ2 exhibited a comparable substrate affinity at a low**
254 **temperature**

255 To date, the affinity between AlgQ2 and alginate oligosaccharides was measured *via* UV
256 absorption difference spectroscopy (Momma *et al*. 2005). However, the method was
257 unsuitable for mtAlgQ2 being cloudy even at room temperature, probably due to protein
258 aggregation. Alternatively, to investigate the molecular state depending on substrate
259 binding, wtAlgQ2 or mtAlgQ2 mixed with 0 or 50 μM of Δ4M was subjected to native
260 PAGE at 4°C (Figure 4a). mtAlgQ2 in the absence of Δ4M demonstrated smear bands,
261 whereas wtAlgQ2 formed a single clear band with a larger migration due to more negative
262 charge. mtAlgQ2 in the absence of the substrate was denatured by the effect of electric
263 field (10 mA, 2 h), whereas wtAlgQ2 maintained its conformation under the same
264 conditions. Because a part of mtAlgQ2 molecules was considered to be spread in a lane

265 or remain a well due to its instability during electrophoresis, mtAlgQ2 showed smear,
266 unclear, and low intensity bands. Although both substrate-bound forms produced a clear
267 protein band at the same position, the substrate-unbound forms appeared at different
268 positions (Figure 4a). These data support the DSF analysis revealing that mtAlgQ2 is
269 stabilized by forming a complex with Δ4M and X-ray crystallography, demonstrating that
270 mtAlgQ2, similar to wtAlgQ2, adopts a closed conformation in the substrate-bound form.
271 wtAlgQ2 and mtAlgQ2 were mixed with various concentrations (0 to 22 μM) of Δ4M
272 and subjected to native PAGE to investigate their alginate-binding ability (Figure 4b).
273 The band intensity corresponding to Δ4M-bound AlgQ2 was quantified. The ratios of the
274 substrate-bound complex formed at each substrate concentration were plotted (Figure 4c).
275 The dissociation constant (K_d) was calculated by fitting isotherms to the Langmuir
276 equation (Langmuir 1918). The K_d of mtAlgQ2 (4.2 μM) was comparable with that of
277 wtAlgQ2 (7.0 μM). This result was supported by the K_d (2.8–15 μM) of wtAlgQ2 for
278 alginate oligosaccharides previously determined *via* UV absorption difference
279 spectroscopy (Momma *et al*. 2005). The local destabilization of the EF-hand-like motif
280 in calcium-unbound AlgQ2 seems not to affect alginate binding.

281 **Induction of ATPase activity through the formation of a complex with mtAlgQ2 and**
282 **AlgM1M2SS**

283 Alginate-bound AlgQ2 interacts with AlgM1M2SS to induce ATPase activity by AlgS
284 (Momma *et al*. 2000; Kaneko *et al*. 2017). The reconstituted AlgM1M2SS ATPase
285 activity in liposomes was measured in the presence or absence of AlgQ2 or substrate
286 (Figure 5a). The AlgM1M2SS-unbound liposome yielded negligible ATPase activity in
287 the presence of AlgQ2 (wtAlgQ2 or mtAlgQ2) and substrate Δ4M. The AlgM1M2SS
288 ATPase activity in liposomes was enhanced by combining AlgQ2 (wtAlgQ2 or mtAlgQ2)

289 and Δ4M, whereas the proteoliposome exhibited a basal ATPase activity in the absence
290 of AlgQ2 (wtAlgQ2 or mtAlgQ2) or Δ4M. The enhanced AlgM1M2SS ATPase activity
291 with mtAlgQ2 and wtAlgQ2 in the presence of substrate indicated that Δ4M-bound
292 mtAlgQ2 could form a complex with AlgM1M2SS and induce ATPase activity.

293 The alginate transport activity of AlgM1M2SS in liposomes was measured using
294 pyridylamino-modified Δ4M (PAΔ4M) as a substrate (Figure 5b). In the absence of
295 AlgQ2, no transport activity was observed in the presence or absence of PAΔ4M. The
296 proteoliposome exhibited transport activity in the presence of wtAlgQ2 and PAΔ4M,
297 whereas the alginate transport activity of AlgM1M2SS in the presence of mtAlgQ2 and
298 PAΔ4M was nearly undetectable. This suggests that, distinct from wtAlgQ2, mtAlgQ2
299 cannot promote the conversion of AlgM1M2SS from outward-facing to inward-facing
300 mode (Figure 6). Although, to date, there is no effect on pyridyl amination of the substrate
301 on the assay of ATPase activity (Maruyama *et al*. 2015), the ATPase activity of the
302 proteoliposome in the presence of mtAlgQ2 and PAΔ4M was measured (Figure 5c).
303 mtAlgQ2 exhibited a slight enhancement of the ATPase activity of AlgM1M2SS even
304 with PAΔ4M, whereas wtAlgQ2 significantly induced ATPase activity in the presence of
305 PAΔ4M. ATPase activity in the presence of mtAlgQ2 and PAΔ4M corresponded to the
306 basal level of the AlgQ2-free proteoliposome in the presence of PAΔ4M.

307 Native PAGE of AlgQ2 and PAΔ4M was also performed to examine the binding of
308 wtAlgQ2 and mtAlgQ2 to PAΔ4M (Figure S1). In the case of mtAlgQ2, although the
309 electrophoretic profile changed with the concentration of PAΔ4M, multiple protein bands
310 were observed in a single lane. The total band intensity in each of lanes corresponding to
311 PAΔ4M suggests that the more amounts of mtAlgQ2 were electrophoresed to a lane, but
312 not accumulated in a well, owing to stabilization of mtAlgQ2 by forming a complex with

PAΔ4M. The complex formation of mtAlgQ2 and PAΔ4M was considered to be inhibited by exogenous PA, an artificially added label to the native substrate.

Discussion

ABC importers are categorized based on the structure as type I, II, or III. Important for all ABC importers to transport molecules across the cytoplasmic membrane, types I and II require SBP, whereas type III requires an energy-coupling factor (Rice *et al*. 2014; Oldham *et al*. 2008). AlgM1M2SS is a member of type I and requires SBP (AlgQ1 or AlgQ2) to transport alginate.

A large number (over 500) of SBP structures have been identified and classified into seven clusters (A to G) (Scheepers *et al*. 2016). A newly proposed cluster G consists of five structure-determined proteins: strain A1 AlgQ1 and AlgQ2, *S. pneumoniae* FusA (PDB ID: 5G60) (Culurgioni *et al*. 2017), *Streptobacillus moniliformis* Smon0123 for the import of glycosaminoglycans (PDB ID: 5GUB) (Oiki *et al*. 2017), and extracellular SBP Blon_2351 (PDB ID: 3OMB) from *Bifidobacterium longum* subsp. *infantis* (unpublished). All SBPs in cluster G have an EF-hand-like motif to bind calcium or magnesium and a relatively large molecular size. Moreover, the EF-hand-like motif is conserved in the primary structures of numerous structure-undetermined SBPs, suggesting that there may be more SBPs belonging to cluster G.

The crystal structures of calcium-bound SBPs from *Thermus thermophiles* HB8 and *Synechocystis* PCC 6803 for the transport of lactic acid and bicarbonate have been solved, although both SBPs have no EF-hand-like motif. Calcium bound to *T. thermophiles* SBP is easily removed by ethylenediaminetetraacetate, and the calcium-unbound SBP remains stable (Akiyama *et al*. 2009). In these SBPs, calcium is coordinated by amino acid

residues and a substrate. Therefore, calcium is incorporated with a substrate or a cofactor (Koropatkin *et al*. 2007). However, calcium bound to the EF-hand-like motif is independent of interactions between AlgQ2 and a substrate, as shown by X-ray crystallography (Figure 1c) and native PAGE (Figure 4a).

In the case of another member in cluster G, FusA, calcium bound to the EF-hand-like motif stabilizes local structure, and this EF-hand-like motif loop is suggested to directly interact with FusB (Culurgioni *et al*. 2017). FusB is the TMD of a fructooligosaccharide-importing ABC transporter based on our crystal structure of AlgM1M2SS in complex with AlgQ2. The stabilization of the EF-hand-like motif loop by calcium is likely responsible for the interaction between Glu221 of FusA and Arg59 of FusB (residue numbers) based on the sequences registered in the database (sp_1797 and sp_1798) and differ from the numbers used previously. Therefore, calcium at the EF-hand-like motif is considered important for substrate transport due to the interaction between the closed conformation of SBP and the inward-facing ABC transporter (Culurgioni *et al*. 2017). On the other hand, no significant interaction between residues of the EF-hand-like motif in closed AlgQ2 and inward-facing AlgM1M2 was observed (Figure 1a). In fact, substrate Δ4M-bound mtAlgQ2 interacted with AlgM1M2SS to induce ATPase activity (Figure 5a), indicating that calcium bound to the EF-hand-like motif is independent of interaction between closed AlgQ2 and inward-facing AlgM1M2SS.

S. pneumoniae producing FusA with a mutated EF-hand-like motif cannot grow on nystose minimal medium, although the mutant FusA maintains affinity with fructooligosaccharides at 25°C. In the case of strain A1, the apparent T_m of mtAlgQ2 was less than 25°C (Figure 3), suggesting that calcium-binding restriction causes global destabilization of substrate-unbound AlgQ2. Since strain A1 is a medium-temperature

361 bacterium showing optimum growth at around 35°C, this destabilization of substrate-
362 unbound SBP is considered lethal for strain A1 in an alginate-minimal medium. The
363 mutation caused local destabilization of the EF-hand-like motif loop in the closed
364 conformation of both AlgQ2 and FusA (Figure 2b) (Culurgioni *et al*. 2017). In the open
365 conformation, calcium bound to EF-hand-like motif in AlgQ2 plays a role in the
366 stabilization of the overall structure, and in the closed conformation, it stabilizes the EF-
367 hand-like motif loop.

368 The substrate transport mechanism of ABC importers has been well studied in
369 $MalFGK_2$, the maltose transporter in *E. coli* and a type I ABC importer (Oldham *et al*.
370 2007; Gould *et al*. 2009; Oldham *et al*. 2013; Bao *et al*. 2015). From the substrate
371 transport scheme proposed in the $MalFGK_2$ and ATPase induction mechanism of
372 AlgM1M2SS (Kaneko *et al*. 2017), the transport of alginate by AlgQ2 and AlgM1M2SS
373 is assumed to involve five (I to V) steps as follows (Figure 6). (I) AlgQ2 binds alginate
374 to form a closed conformation. (II) Substrate-bound AlgQ2 interacts with inward-facing
375 AlgM1M2SS to induce ATPase activity and AlgSs binding of ATP. (III) AlgQ2 and
376 AlgM1M2SS change to outward-facing mode. (IV) AlgQ2 passes alginate to
377 AlgM1M2SS. (V) AlgQ2 liberates from AlgM1M2SS, and AlgM1M2SS changes to
378 inward-facing mode. The enhancement of ATPase activity by mtAlgQ2 in the presence
379 of substrate Δ4M suggests that the conformational change occurs from inward- to
380 outward-facing mode in the TMD (AlgM1M2) and from open to closed conformation in
381 the NBD (AlgSS). With PAΔ4M substrate, no transport activity was detected because
382 PAΔ4M is unsuitable for inducing ATPase activity by mtAlgQ2, suggesting that the
383 transport procedure stops at step I.

384 In conclusion, calcium bound to the EF-hand-like motif is crucial for stabilizing

substrate-unbound AlgQ2 in the open conformation, especially at temperatures greater than 25°C, not for the direct interaction between substrate-bound AlgQ2 in the closed conformation and inward-facing AlgM1M2SS. Finally, this demonstrates that calcium bound to AlgQ2 is essential for alginate import at strain A1-growing temperature.

Supplementary material

Supplementary material is available at *Bioscience, Biotechnology, and Biochemistry* online.

Data availability

The data underlying this article will be shared on reasonable request to the corresponding author.

Author contribution

K. O and Y. M. performed the experiments. K. O., Y. M., R. T., B. M, K. M., and W. H. analyzed the data. Y. M. and W. H. designed the study. K. O., Y. M., R. T., and W. H. wrote the manuscript.

Acknowledgments and Funding

We thank Prof. Martin A. Walsh (Deputy Director at Diamond Light Source in UK, Research Complex at Harwell, Harwell Science and Innovation Campus in UK) for his supports of our study. We also thank Drs. S. Baba and N. Mizuno of the Japan Synchrotron Radiation Research Institute (JASRI) for their kind help in data collection. Diffraction data were collected at beamline BL38B1 of SPring-8 (Hyogo, Japan) with the approval

409 of JASRI (projects 2017B2592, 2016B2574, and 2016A2574). The authors would like to
410 thank Enago (www.enago.com) for the English language review.
411 This work was supported in part by Grants-in-Aid for Scientific Research from the
412 Japanese Society for the Promotion of Science (W. H.) and by a research grant from The
413 Yanmar Environmental Sustainability Support Association (W. H.).
414

415 **Disclosure statement**

416 No potential conflict of interest was reported by the authors.
417

418 **References**

419 Ababou A, and Zaleska M. Electrostatics effects on Ca^{2+} binding and conformational
420 changes in EF-hand domains: Functional implications for EF-hand proteins. *Arch*
421 *Biochem Biophys* 2015;**587**:61-69.
422 Akiyama N, Takeda K, and Miki K. Crystal structure of a periplasmic substrate-binding
423 protein in complex with calcium lactate. *J Mol Biol* 2009;**392**:559-65.
424 Bao H, Dalal K, Cytrynbaum E *et al*. Sequential action of MalE and maltose allows
425 coupling ATP hydrolysis to translocation in the MalFGK2 transporter. *J Biol Chem*
426 2015;**290**:25452-60.
427 Berntsson R P, Smits S H, Schmitt L *et al*. A structural classification of substrate-binding
428 proteins. *FEBS Lett* 2010;**584**:2606-17.
429 Carafoli E. Calcium signaling: a tale for all seasons. *Proc Natl Acad Sci U S A*
430 2002;**99**:1115-22.
431 Chifflet S, Torriglia A, Chiesa R *et al*. A method for the determination of inorganic
432 phosphate in the presence of labile organic phosphate and high concentrations of

protein: application to lens ATPases. *Anal Biochem* 1988;**168**:1-4.

Culurgioni S, Harris G, Singh A K *et al*. Structural basis for regulation and specificity of fructooligosaccharide import in *Streptococcus pneumoniae*. *Structure* 2017;**25**:79-93.

Davidson A L, Dassa E, Orelle C *et al*. Structure, function, and evolution of bacterial ATP-binding cassette systems. *Microbiol Mol Biol Rev* 2008;**72**:317-64.

Delfina C D, Manita G, and Marianna P. Calcium binding proteins and calcium signaling in prokaryotes. *Cell Calcium* 2015;**57**:151-65.

Emsley P, and Cowtan K. Coot: model-building tools for molecular graphics. *Acta Crystallogr D Biol Crystallogr* 2004;**60**:2126-32.

Gacesa P. Alginates. *Carbohydr. Polym.* 1998;**8**:161-82.

Gifford J L, Walsh M P, and Vogel H J. Structures and metal-ion-binding properties of the Ca^{2+}-binding helix-loop-helix EF-hand motifs. *Biochem J* 2007;**405**:199-221.

Gould A D, Telmer P G, and Shilton B H. Stimulation of the maltose transporter ATPase by unliganded maltose binding protein. *Biochemistry* 2009;**48**:8051-61.

Hisano T, Kimura N, Hashimoto W *et al*. Pit structure on bacterial cell surface. *Biochem Biophys Res Commun* 1996;**220**:979-82.

Kaneko A, Uenishi K, Maruyama Y *et al*. A solute-binding protein in the closed conformation induces ATP hydrolysis in a bacterial ATP-binding cassette transporter involved in the import of alginate. *J Biol Chem* 2017;**292**:15681-90.

Koropatkin N M, Koppenaal D W, Pakrasi H. B *et al*. The structure of a cyanobacterial bicarbonate transport protein, CmpA. *J Biol Chem* 2007;**282**:2606-14.

Langmuir I. The adsorption of gases on plane surfeces of glass, mica and plantinum. *J Am Chem Soc* 1918;**40**:1361-1403.

Laskowski R A, Macarthur M W, Moss D S *et al*. Procheck - a program to check the

457 stereochemical quality of protein structures. *J Appl Crystallogr* 1993;**26**:283-91.
458 Locher K P. Structure and mechanism of ATP-binding cassette transporters. *Philos Trans*
459 *R Soc Lond B Biol Sci* 2009;**364**:239-45.
460 Maruyama Y, Itoh T, Kaneko A *et al*. Structure of a bacterial ABC rransporter involved
461 in the import of an acidic polysaccharide alginate. *Structure* 2015;**23**:1643-54.
462 McLellan T. Electrophoresis buffers for polyacrylamide gels at various pH. *Anal Biochem*
463 1982;**126**:94-9.
464 Momma K, Mikami, B Mishima Y *et al*. Crystal structure of AlgQ2, a macromolecule
465 (alginate)-binding protein of *Sphingomonas* sp. A1 at 2.0Å resolution. *J Mol Biol*
466 2002;**316**:1051-59.
467 Momma K, Mishima Y, Hashimoto W *et al*. Direct evidence for *Sphingomonas* sp. A1
468 periplasmic proteins as macromolecule-binding proteins associated with the ABC
469 transporter: molecular insights into alginate transport in the periplasm. *Biochemistry*
470 2005;**44**:5053-64.
471 Momma K, Okamoto M, Mishima Y *et al*. A novel bacterial ATP-binding cassette
472 transporter system that allows uptake of macromolecules. *J Bacteriol* 2000;**182**:3998-
473 4004.
474 Murshudov G N, Vagin A A, and Dodson E J. Refinement of macromolecular structures
475 by the maximum-likelihood method. *Acta Crystallogr D Biol Crystallogr*
476 1997;**53**:240-55.
477 Niesen F H, Berglund H, and Vedadi M. The use of differential scanning fluorimetry to
478 detect ligand interactions that promote protein stability. *Nat Protoc* 2007;**2**:2212-21.
479 Nishitani Y, Maruyama Y, Itoh T *et al*. Recognition of heteropolysaccharide alginate by
480 periplasmic solute-binding proteins of a bacterial ABC transporter. *Biochemistry*

2012;**51**:3622-33.

Oiki S, Mikami B, Maruyama Y *et al*. A bacterial ABC transporter enables import of mammalian host glycosaminoglycans. *Sci Rep* 2017;**7**:1069.

Oldham M L, Chen S, and Chen J. Structural basis for substrate specificity in the *Escherichia coli* maltose transport system. *Proc Natl Acad Sci U S A* 2013;**110**:18132-7.

Oldham M L, Davidson A L, and Chen J. Structural insights into ABC transporter mechanism. *Curr Opin Struct Biol* 2008;**18**:726-33.

Oldham M L, Khare D, Quiocho F A *et al*. Crystal structure of a catalytic intermediate of the maltose transporter. *Nature* 2007;**450**:515-21.

Otwinowski Z, and Minor W. Processing of X-ray diffraction data collected in oscillation mode. *Methods Enzymol* 1997;**276**:307-26.

Rice A J, Park A, and Pinkett H W. Diversity in ABC transporters: type I, II and III importers. *Crit Rev Biochem Mol Biol* 2014;**49**:426-37.

Scheepers G H, Lycklama A N J A, and Poolman B. An updated structural classification of substrate-binding proteins. *FEBS Lett* 2016;**590**:4393-401.

Schneider C A, Rasband W S, and Eliceiri K W. NIH image to ImageJ: 25 years of image analysis. *Nat Methods* 2012;**9**:671-5.

Schrodinger L L C The PyMOL Molecular Graphics System, version 1.3r1. 2010.

Standley D M, Toh H, and Nakamura H. Detecting local structural similarity in proteins by maximizing number of equivalent residues. *Proteins* 2004;**57**:381-91.

Tang C, Schwieters C D, and Clore G M. Open-to-closed transition in apo maltose-binding protein observed by paramagnetic NMR. *Nature* 2007;**449**:1078-82.

ter Beek J, Guskov A, and Slotboom D J. Structural diversity of ABC transporters. *J Gen*

505 *Physiol* 2014;**143**:419-35.

506 Toh H. Introduction of a distance cut-off into structural alignment by the double dynamic

507 programming algorithm. *Comput Appl Biosci* 1997;**13**:387-96.

508 Vagin A, and Teplyakov A. MOLREP: an automated program for molecular replacement.

509 *J Appl Crystallogr* 1997;**30**:1022-5.

Table1. Calcium content of purified AlgQ2

	Ca (μM)	(Ca mol)/(protein mol)
wtAlgQ2	11	1.1
mtAlgQ2	1.7	0.17

510

511

Table 2. Data collection and refinement statistics

Data collection	
Wavelength (Å)	1.00000
Resolution range (Å)	50.0–2.20 (2.24–2.20) [a]
Space group	*P*1
Unit-cell parameters (Å, °)	
a, b, c	45.87, 60.82, 87.23
α, β, γ	80.37, 89.81, 88.17
Total observations	124992 (5993)
Unique reflections	47003 (2305)
Completeness (%)	97.8 (97.9)
$I/\sigma(I)$	63.6 (5.5)
R_{merge}	0.145 (0.362)
R_{mean}	0.178 (0.452)
$CC_{1/2}$	0.821
Wilson B ($Å^2$)	29.6
Refinement	
Resolution range (Å)	50.0-2.20 (2.26-2.20)
R_{work}/R_{free}	0.210 (0.268)/0.271 (0.336)
Protein molecules/ASU	2
No. atoms	
Protein	7974
Saccharide	72
Calcium ion	0
Water molecule	200
RMSD	
Bond lengths (Å)	0.012
Bond angles (deg.)	1.517
Ramachandran plot	
Most favored (%)	97.3
Allowed (%)	2.3
Outlier (%)	0.4
PDB ID	6JHX

[a] The highest resolution shell is shown in parentheses.

Table 3. Apparent T_m (°C)

	No ligand (T_{open})	$CaCl_2$ (T_{open})	Δ4M (T_{closed})	$CaCl_2$+Δ4M (T_{closed})
wtAlgQ2	45.63	45.63	63.18	63.18
mtAlgQ2	<25	<25	55.72	55.72

514

515

Figure legends

Figure 1. X-ray crystal structures of ABC transporter and AlgQ2. (a) (Left) The complex structure of AlgQ2 and AlgM1M2SS (PDB ID: 4TQU). Magenta, AlgQ2; green, AlgM1; cyan, AlgM2; orange, AlgS. Calcium ion in AlgQ2 is indicated by a yellow ball. (Right) Magnified image at the interface between AlgQ2 and AlgM2. (b) EF-hand-like calcium-binding site of AlgQ2. (c) calcium (yellow ball) is far from the substrate (red/white balls)-binding site of AlgQ2.

Figure 2. X-ray crystal structure of mtAlgQ2. (a) Overall structure of mtAlgQ2. Gray and red-colored sticks indicate unsaturated alginate trisaccharide. (b) (Left) Structure of mutated EF-hand-like motif. Red, EF-hand-like motif helix; green, loop. (Right) The figure shows the $2F_o$-F_c map contoured at 1.2 σ around the EF-hand-like motif. (c) Superimposing of wtAlgQ2 and mtAlgQ2 for all Cα atoms. Blue, mtAlgQ2; orange, wtAlgQ2. Calcium ion is indicated by a yellow ball.

Figure 3. Thermal shift assay by DSF. Top, fluorescent profile. Bottom, negative derivative curve plot of the fluorescent profile. Red, wtAlgQ2 without Δ4M; blue, mtAlgQ2 without Δ4M; black, wtAlgQ2 with Δ4M; green, mtAlgQ2 with Δ4M.

Figure 4. Native PAGE profile of AlgQ2. (a) wtAlgQ2 or mtAlgQ2 with or without 50-μM Δ4M. (b) Binding ability of wtAlgQ2 (upper) and mtAlgQ2 (lower) to Δ4M in proportion to increasing substrate concentration. (c) Profile of formation of AlgQ2 and Δ4M complex. Circle; wtAlgQ2, square; mtAlgQ2.

Figure 5. ATPase and transport activity of AlgM1M2SS. (a) ATPase activity in the presence (+) or absence (−) of each component in the reaction mixture. ATPase activity was represented as phosphate (nmol) produced by 1-mg AlgM1M2SS per 1 min. (b) Transport activity. Transport activity used PAΔ4M as a substrate in the presence (+) or

absence (−) of each component in the reaction mixture. Activity of AlgM1M2SS in the presence of wtAlgQ2 was taken as 100%. Negative values indicate no transport activity calculated by subtraction of the mean values of the observed transport activity in liposomes without AlgM1M2SS. (c) ATPase activity using PAΔ4M as a substrate in the presence (+) or absence (−) of each component in the reaction mixture. Assays were performed three times, and the error bars represent SE.

Figure 6. Mechanistic model of ABC transporter for alginate import. The dynamics of ABC transporter machinery model. Pink, wtAlgQ2; purple, mtAlgQ2; light yellow, calcium; gray, alginate; green, AlgM1; blue, AlgM2; dark yellow, AlgS.

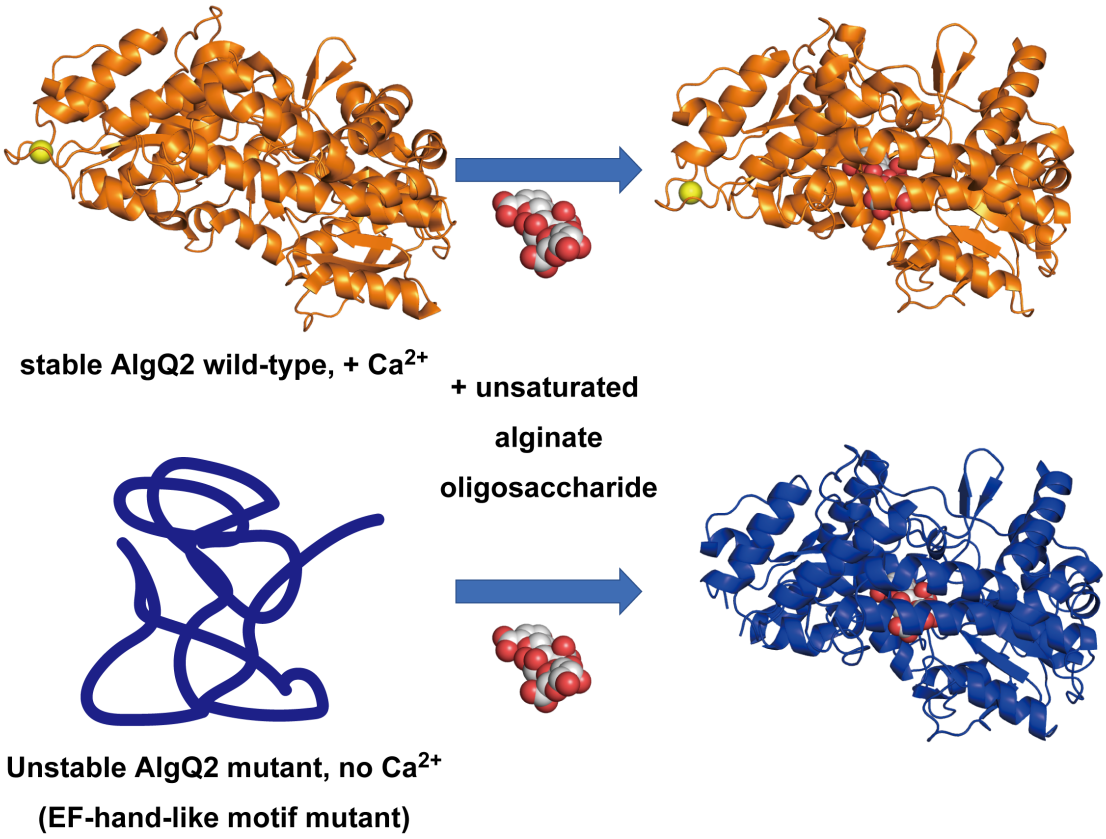

551

552 **Graphical abstract.** The calcium bound to EF-hand-like motif stabilizes the substrate-
553 unbound AlgQ2, while calcium-free AlgQ2 adopts a closed conformation in complex
554 with substrate.

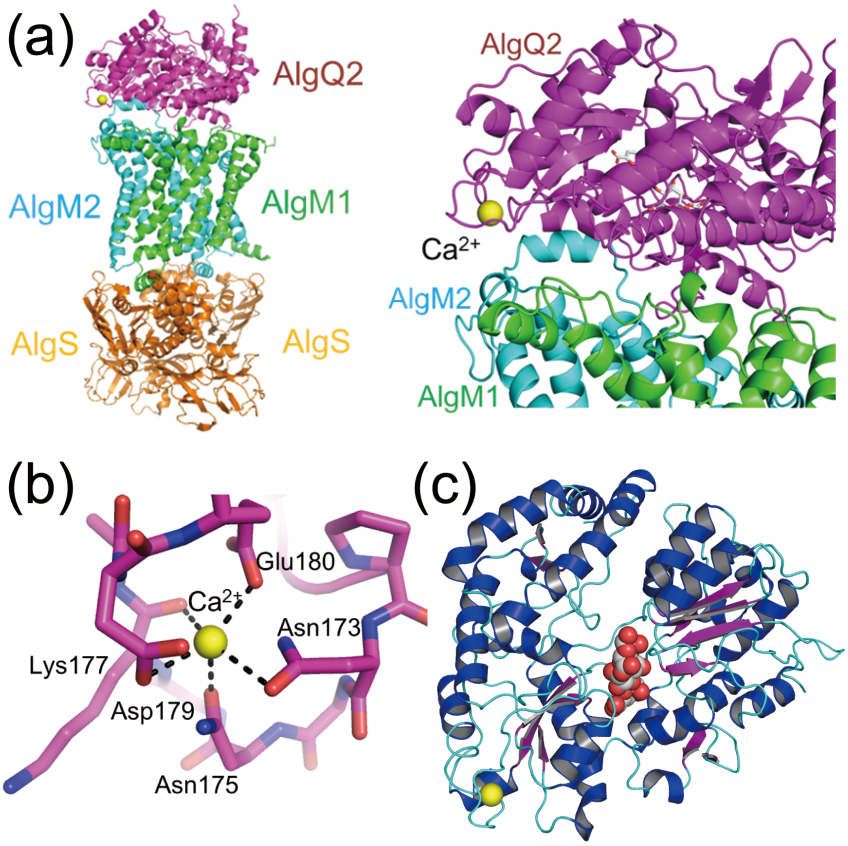

555

556 **Figure 1.**

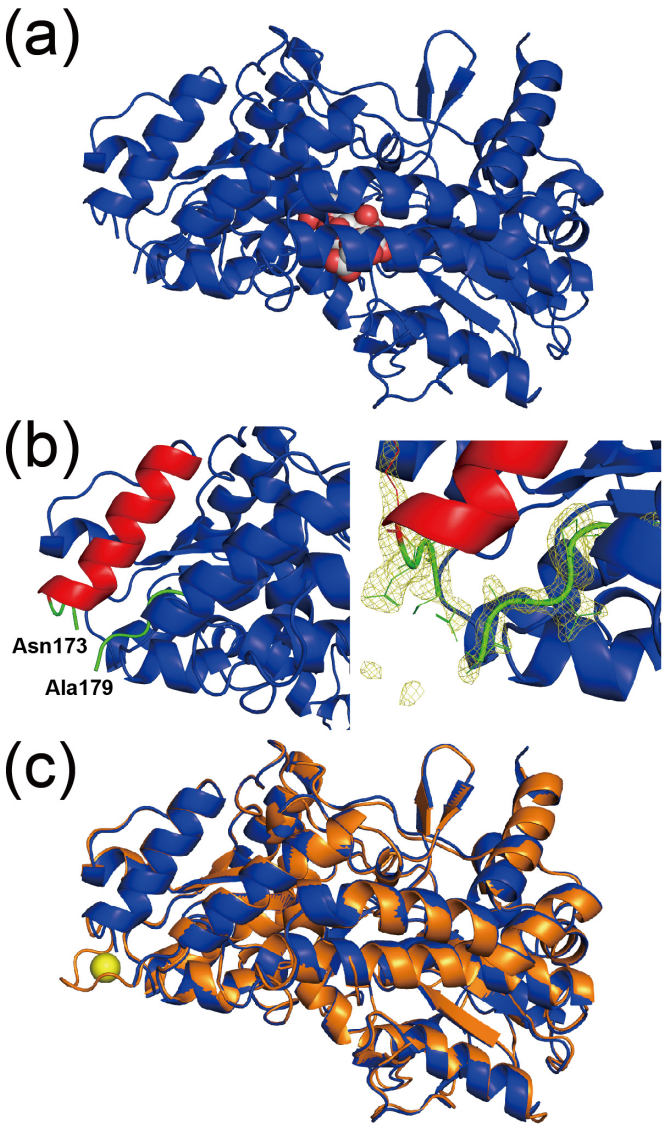

Figure 2.

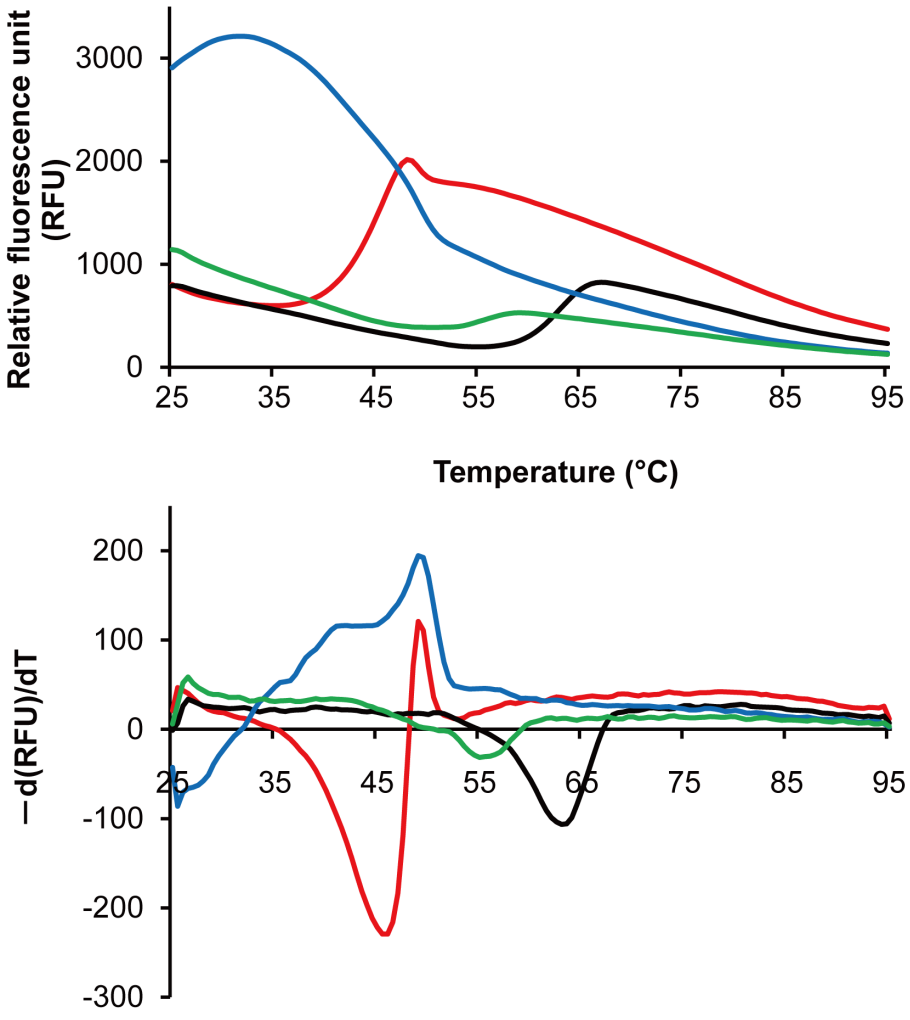

561

562 **Figure 3.**

563

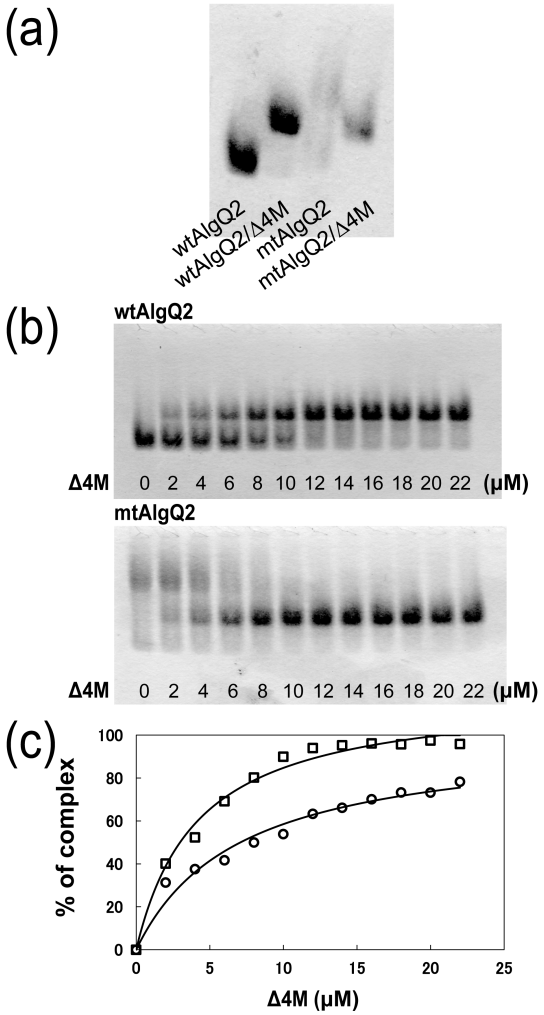

564

565 **Figure 4.**

566

567

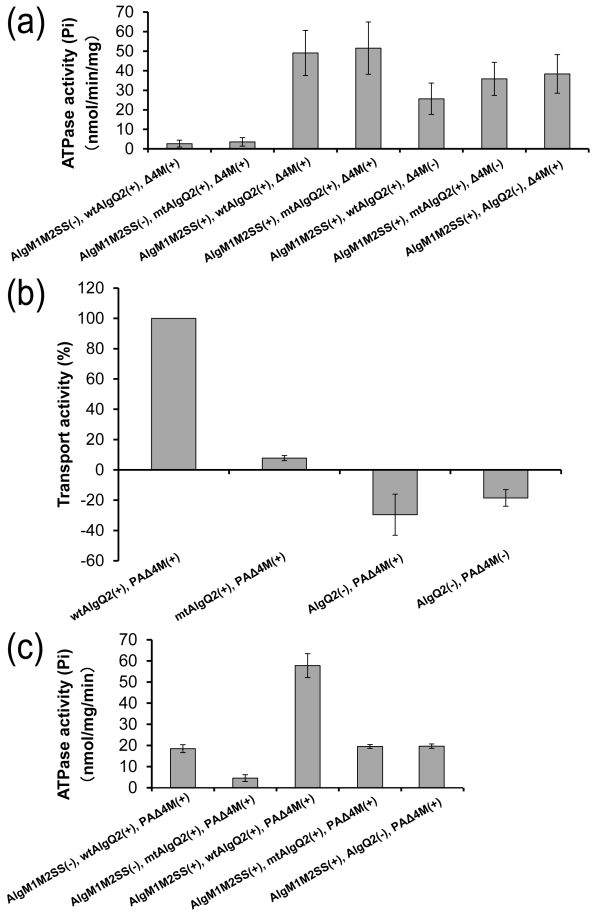
(a)
ATPase activity (Pi)
(nmol/min/mg)
70
60
50
40
30
20
10
0
AlgM1M2SS(-), wtAlgQ2(+), Δ4M(+)
AlgM1M2SS(-), mtAlgQ2(+), Δ4M(+)
AlgM1M2SS(+), wtAlgQ2(+), Δ4M(+)
AlgM1M2SS(+), mtAlgQ2(+), Δ4M(+)
AlgM1M2SS(+), wtAlgQ2(+), Δ4M(-)
AlgM1M2SS(+), mtAlgQ2(+), Δ4M(-)
AlgM1M2SS(+), AlgQ2(-), Δ4M(+)
(b)
Transport activity (%)
120
100
80
60
40
20
0
-20
-40
-60
wtAlgQ2(+), PAΔ4M(+)
mtAlgQ2(+), PAΔ4M(+)
AlgQ2(-), PAΔ4M(+)
AlgQ2(-), PAΔ4M(-)
(c)
ATPase activity (Pi)
(nmol/mg/min)
70
60
50
40
30
20
10
0
AlgM1M2SS(-), wtAlgQ2(+), PAΔ4M(+)
AlgM1M2SS(-), mtAlgQ2(+), PAΔ4M(+)
AlgM1M2SS(+), wtAlgQ2(+), PAΔ4M(+)
AlgM1M2SS(+), mtAlgQ2(+), PAΔ4M(+)
AlgM1M2SS(+), AlgQ2(-), PAΔ4M(+)

Figure 5.

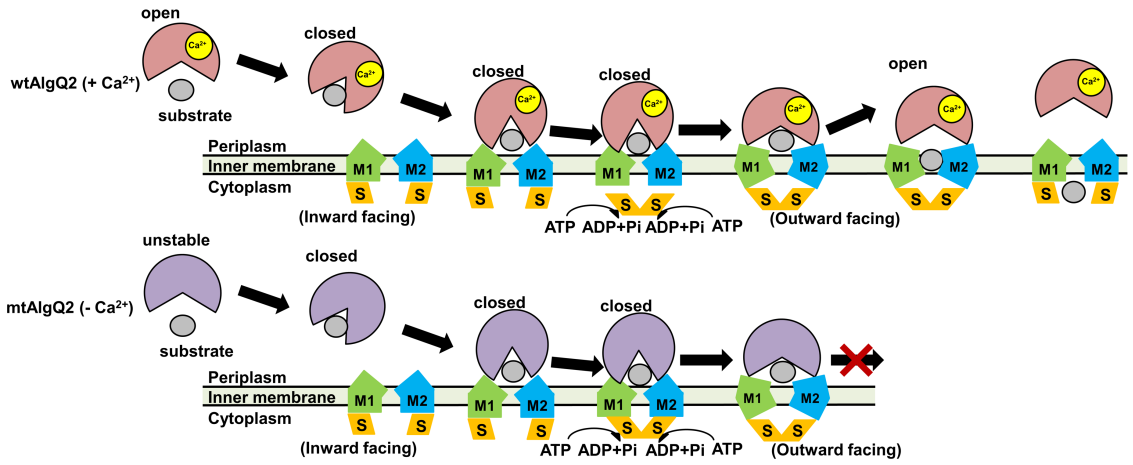

572

573 **Figure 6.**

574

575

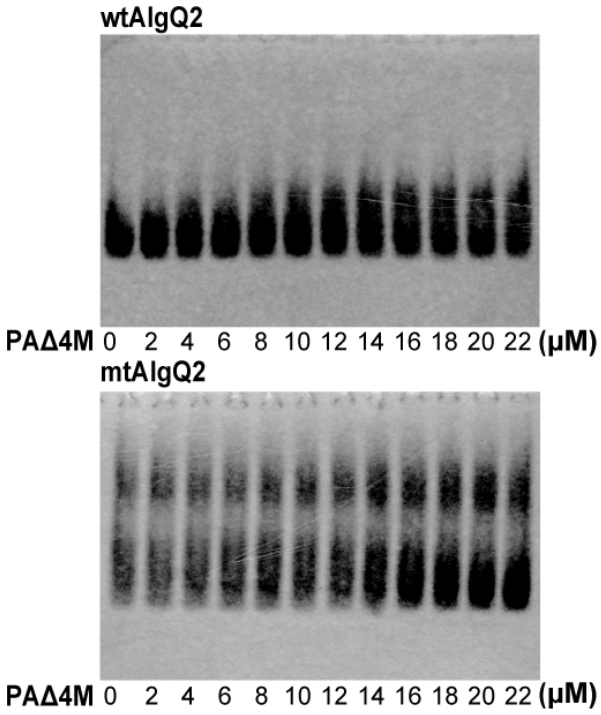

576

577 **Figure S1.** PAΔ4M-binding ability of wtAlgQ2 and mtAlgQ2 with increasing PAΔ4M
578 concentration. Top, wtAlgQ2; bottom, mtAlgQ2. The difference in the band profile from
579 Figure 4b was thought to be due to positive-charge donated by PA.

580

581